Impact of soil water content on the overturning resistance of young Pinus Pinaster in sandy soil

Pauline Défossez, G. Veylon, M. Yang, Jean-Marc Bonnefond, Didier Garrigou, P. Trichet, Frédéric Danjon

Impact of soil water content on the overturning resistance of young *Pinus Pinaster* in sandy soil

P. Défossez[a,*], G. Veylon[b], M. Yang[a], J.M. Bonnefond[a], D. Garrigou[a], P. Trichet[a], F. Danjon[c]

[a] *INRAE, Bordeaux Sciences Agro, ISPA, F-33882, Villenave d'ornon, France*
[b] *INRAE, Aix Marseille Univ., RECOVER, F-13182, Aix-en-Provence, France*
[c] *INRAE, Univ. Bordeaux, BIOGECO, F-33610, Cestas, France*

Abstract

Background and aims. The tree resistance to uprooting is crucial to face wind damage in temperate forest. Tree anchorage varies considerably with site conditions, species, and tree age. Only few studies have focused on the influence of the site soil properties on the tree anchorage. With ongoing climate change, the soil hydrologic conditions are changing in Europe due to higher precipitations during winter, with possible higher risk of wind damage in forests.

Methods. This study investigates the role of soil hydrology on tree anchorage of *Pinus pinaster* in sandy soil with a combination of field experiments and simulations. Tree pulling experiments until root-soil system failure were performed for 12 *Pinus pinaster* of 14 years-old growing in podzol to measure the tree resistance to uprooting M_c for two contrasted soil water conditions. In addition, simulations were conducted to analyze how M_c changes during the progressive wetting of the layered soil. For that purpose, a new model was developed for M_c. This model also includes a sub-model for the shear mechanical strengths of the sandy soil layers and their variation with soil water content. The model was calibrated with different data sets: (1) the M_c-data obtained from the tree pulling experiments performed on 14 years-old *Pinus pinaster*; (2) the 3D root system architectures of the pulled trees ; and (3) the soil shear

*Corresponding Author.
Tel.: +33 (0)5 57 12 23 64.
Email address: pauline.defossez@inrae.fr (P. Défossez)

mechanical strength as function of the soil water content measured in laboratory by direct shear tests and soil water retention curve measurements. After calibration, M_c-calculations were performed when simulating a progressive soil wetting by water table increase or by water saturation front progression.

Results. Field-data and simulations show that M_c depends little on soil water content outside the domain of complete soil saturation. Close to saturation, simulations show that M_c decreases drastically up to % 40 of its value. This is specific to sandy soil whose mechanical strength is mainly due to the capillarity forces between grains. As illustrated by simulations, the anchorage resistance results from two components. The first friction component slightly increases with soil water content. The second suction component decreases little with soil water content and drops down at saturation when all the interstitial water in the soil porous network merges.

Conclusions. This loss of anchorage resistance at full saturation may increase considerably the risk of wind damage of forest growing in sandy soil as floods increase with climate change in Europe.

Keywords: Windstorm damage, Toppling, Soil water content, Anchorage, Soil shear strength, Pinus pinaster, sandy soil

1. Introduction

Wind damage represents more than 50% by timber volume of the forest damage in Europe (Schelhaas, 2008). Storm damage has considerable consequences for the forest economy, and the ecological functioning and survival of European forests (Lindroth et al., 2009; Seidl et al., 2014). The increasing stock and average age of European forests and the observed on–going climate changes, with the prediction of stronger wind storms (Della-Marta and Pinto, 2009), can also lead to a growing wind risk. For instance, storm Klaus which hit southern

Europe in January 2009 resulted in an estimated 43 million m^3 of timber being blown down in Southwest France, including a volume of 37 million m^3 for Pinus pinaster (GPMF, 2011). In Europe, most of the damage are from tree overturning (Gardiner et al., 2016).

Different authors suggested that soil properties can impact the tree anchorage (Coutts, 1986; Ennos, 2000; Dupuy et al., 2007; Gardiner et al., 2010, 2016). The soil texture (clay or sandy soil) was established to be an important factor (Moore, 2000; Nicoll et al., 2006). With climate change, storms tend to be accompanied by heavier rainfall in Europe leading to more saturated soils (Stocker et al., 2014) with possible higher risk of wind damage. But to date, data on these effects remain scarce. Only Kamimura et al. (2012) investigated the stability of 30 year old hinoki trees under various irrigation treatments to recreate the soil conditions during typhoon. They found that high soil water content below the soil-root plate tends to decrease the tree stability. Kamimura et al. (2012) did not establish an explicit relation with the soil mechanical strength so that the role of the soil water content has not yet been clarified.

The soil shear mechanical properties of the rhizosphere have been extensively analyzed in the context of slope stability with vegetation (Stokes et al., 2008; Genet et al., 2008; Schwarz et al., 2010; Genet et al., 2010; Wu, 2013). The decrease in soil shear strength with rainfall-induced wetting has been largely recognized to trigger soil slope sliding. Numerous authors took into account for this phenomena to predict slope stability as function of climate conditions (Simon and Collison, 2002; Osman and Barakbah, 2006; Pollen, 2007; Fan and Su, 2009; Rahardjo et al., 2014; Veylon et al., 2015; Gonzalez-Ollauri and Mickovski, 2017; Yang et al., 2017; Hales and Miniat, 2017; Kim et al., 2017). This assumption was extended to the problematic of tree stability under wind and it is generally accepted that soil wetting decreases the tree anchorage strength and the tree stability (Coutts, 1986; Ennos, 2000; Moore, 2000; Gardiner et al., 2010, 2016).

Most of knowledge about the role of the soil mechanical strength on the tree anchorage has come from numerical studies. Following the pioneer work of Blackwell et al. (1990), numerical models have been developed to estimate the tree resistance to overturning (Dupuy et al., 2005; Rahardjo et al., 2009; Yang et al., 2014, 2018). Models based on the finite element method (FEM) describe independently the root architecture as a ramified structure of beams and the soil as a continuous medium defined by the laws of soil mechanics. Interestingly, they provide a method to differentiate the effects caused by the root architecture from those caused by the soil resistance. Parametric studies with FEM models were conducted to examine the impact of soil shear properties on the tree stability (Yang et al., 2018; Dupuy et al., 2005, 2007; Rahardjo et al., 2009). In these last numerical studies, the laws used for soils do not account for soil water. Only few authors examined the effect of change in soil water content on the tree stability. Rahardjo et al. (2009) and Rahardjo et al. (2017) proposed to account for the influence of soil hydrology for clay soils and predicted a systematic decrease in tree anchorage with an increase in the soil wetting. These last simulations were not corroborated by observations. In addition all these numerical studies describe ideal soils or simplified root system where the interaction between roots and surrounding soil are highly simplified.

The goal of this paper is to better understand the role of the soil mechanical strength on the tree anchorage and how it changes with soil water content. We focus on *P. pinaster* cultivated on a sandy soil that is representative of the Landes de Gascogne Forest (France). The Landes de Gascogne Forest covers 1 million hectares in south-western France and has been heavily damaged by winter windstorms over the last 20 least years. This study investigates changes in the tree anchorage of young *P. pinaster* with soil wetting induced by rainfall. Our approach combines field-data and simulations to better understand the evolution of the tree stability with the progressive redistribution of water within the different soil horizons :

1. field pulling experiments were performed to measure the tree anchorage resistance in wet and very wet soil conditions;
2. a new anchorage model was developed including a detailed description of the root system properties and the soil properties in the different soil horizons. We implemented in this model a sub-model dedicated to evaluate the soil mechanical strength as a function of the distribution of water between soil horizons. This new model allows for simulating the tree resistance to uprooting in situations where all soil horizons reach saturation when experiments are technically difficult to be conducted.
3. different simulations of the tree anchorage resistance were performed as the soil layers become saturated with soil wetting. Prior simulations, the model was calibrated from (i) the field tree pulling-data (ii) laboratory-data for the 3D root system architecture of the pulled trees (iii) laboratory-data for the soil shear mechanical properties as function of the soil water content corresponding to the field pulling experiment.

2. Materials and Methods

2.1. Field-data for the tree resistance to overturning

Site description. The experimental site is located in the Landes de Gascogne Forest (Nézer forest in the southwest of France, altitude 15 m, latitude $44.6448^o N$, longitude $-1.03333^o W$; city of Teich). The site is a medium humid sandy spodosol with a discontinuous deep hard pan at 40-90 cm depth (Augusto et al.

2010). Topography is flat (average slope less than 2%). The climate is temperate marine, with moderately warm summers and cool wet winters. Mean annual rainfall is 945 mm, mean annual temperature is 13.8^oC, and prevailing winds and storm winds come from the West (Météo France – 1981-2010). The water table fluctuates close to the soil surface during rainy winters, but sinks to 1.5 m depth in late summer.A major storm damaged the stands on 23 January 2009 with 18% toppled in the seeded stand and 30% in the planted stand. 12 straight trees (6 were seeded and 6 were planted) with the same development stage and without any stem fork were selected. Stem Diameter at Breast Height (DBH) varied between 16.23 and 19.09 cm and height between 9.38 and 11.65 m (Table 1). These trees represent a subsample of the 48 trees studied by Danquechin Dorval et al. (2016) who established their 3D root system architecture as detailed in the following.

Soil type. The soil of the experimental site was characterized by its particle size distribution (Figure 1). This distribution was performed on three samples by sedimentation and sieving to determine the particles diameters D_{10}, D_{50}, D_{60} corresponding respectively to 10%, 50% and 60% of passing. Soil foundation was composed of medium sand with a median particle size D_{50}=0.40 mm and a coefficient of uniformity $C_u = D_{60}/D_{10}$=3. The grains shape was characterized as rounded particles with medium sphericity and the fine content less than 5%. Soil particle density ρ_s=2.60 Mg m^{-3} was measured for each horizon (0-10, 10-40 and 40-60 cm) by water Pycnometer following the procedure ASTM D 854 – 02. The loosest and densest state of the soil were characterized by the maximum e_{max} and minimum e_{min} void ratios with $e=\frac{\rho_s}{\rho_d}-1$, ρ_d being the soil dry bulk density. e_{min}=0.50 and e_{max}=0.85 were estimated from D_{50} based on published formula (Cubrinovski and Ishihara, 2002; Patra et al., 2010). The total carbon content was measured by dry combustion in a CHN autoanalyser

(Carlo Erba NA 1500). The organic carbon content varied from 2.5 to 1% with soil horizon depth (0-10 to 40-60 cm).

Field pulling tests. In order to measure the effects of soil water content on the tree overturning resistance, pulling tests were performed at two contrasted soil water content conditions. A first series of tests was performed in April 2012 during a period of rain with a water table at about 60 cm depth. In this series, three soil horizons (0-10, 10-40 and 40-60 cm) were wet and unsaturated. A second series was performed in February 2013 after a period of heavy rain with a water table around 40 cm. In this second series, both first horizons were very wet and unsaturated and the horizon (40-60 cm) was saturated .

The procedure for the tree pulling experiments was based on Nicoll et al. (2006) and depicted in Fig. 4. In 2012 (04/23 and 04/24) and in 2013 (01/30 and 02/01) 12 trees were pulled until failure. The tops of the trees were removed, leaving 3 m high stem to eliminate the contribution of the crown load (Coutts, 1986). The selected trees were pulled with a motorised winch (Winchmax, UK, maximal strength capacity 58 kN). The winch was attached to the base of an anchoring tree at a distance to the winched tree (8 to 10 m) and anchored within the soil by two piles dug over a depth of 0.8 m. The height (L) of the cable attachment was low enough on the stem to induce anchorage failure without stem breakage. L varied from tree to tree, from 1.4 m to 1.8 m. The cable attachment was guyed by screws driven through the stem to avoid the slip during pulling tests. Trees were winched perpendicular to tree row lines, planted trees toward East and seeded trees toward North. The pulling force F applied to the winched tree was measured by a load cell (SM 5420, Sensel, France, maximum load 50 kN). Two inclinometers (SN 25276; Sensel, France) were tied to the tree at the cable attachment point and at the base of the stem to measure respectively the tree total rotation α and the rotation of the root-soil system α_r. The load cell and the inclinometers were connected to a computer that recorded data. Both the distance between the tested tree and anchoring point and the distance between the anchoring point and the cable attachment point were measured to estimate θ the angle of the cable from the horizontal.

The turning moment M applied to the tree by the winching apparatus was calculated as followed :

$$M = FL(\cos\theta\cos\alpha + \sin\theta\sin\alpha). \tag{1}$$

We estimated from the $M(\alpha_r)$ curves: (i) the initial stiffness of the root-soil system k_r, deduced from the initial linear part of the moment-rotation curves (Neild and Wood, 1999; Jonsson et al., 2006; Lundström et al., 2007), (ii) the critical turning moment M_c, corresponding to the maximum of the moment-rotation curves, (iii) the critical angle α_r^c corresponding to M_c. M_c characterizes the tree capacity to resist overturning induced by windstorms (Coutts, 1986).

Field soil water content conditions. The degree of soil saturation during pulling tests were deduced from the measurements of the soil gravimetric water content w_n and the soil dry bulk density profiles ρ_d as function of soil depth z. Both w_n and ρ_d were measured by gravimetric method on samples collected the same day as the pulling experiments. Soil samples were collected by cylinders at 5, 20 and 45 cm depth from soil surface in 2012 and at 5 and 20 cm in 2013. In 2013, it was impossible to collect cylinders at larger depth because of soil saturation. Cylinders were of 8 cm height and 5 cm diameter. Four profiles were measured for each tested tree at four points of the compass, at 2 m from the tree stump to capture variability of the soil water content. The saturation degree S_r was deduced as follows:

$$S_r = w_n \frac{\rho_s \rho_d}{\rho_w(\rho_s - \rho_d)} \tag{2}$$

with ρ_w the water density.

Root system characteristics. The analysis of the 3D architecture root systems of the 12 tested trees has been presented in Danquechin Dorval et al. (2016). Root systems were excavated on 15 May 2012 for the first 6 pulled trees and on the 25 February 2013 for the others. Roots were classified in Fig. 3 according to their orientation and position in space. The taproots (T) follow vertical direction and the shallow roots follow horizontal direction and differ if they are in the winch sector (W) or in the counter-winch (CW). In this study, the roots are quantified by their volume V_{root} and by their specific root length (SRL) defined as the ratio between root length and root volume without stump. The finer are roots, the higher SRL is. SRL-values were corrected to avoid a bias due to root end loss during excavation (Danquechin Dorval et al., 2016).

2.2. Model for the tree resistance to overturning

The purpose of this section is to describe the tree resistance to overturning with a model that accounts for the soil mechanical properties and their variation with the soil water content.

Anchorage rupture. This model is based on the observations of overturning performed during the pulling tests. Usually, for large pine, the root-soil system exhibits a large root-soil plate where soil is very dense and where soil is embedded in a root cage (Danjon et al., 2005). Large trees present a massive and dense root-soil plate that tilts as a block during the overturning failure. For smaller trees, like those studied here, there is no such a cage (Danquechin Dorval et al., 2016). Here, the winching tests showed that failure occurs by mixed mode of ruptures: the ruptures of roots them-self usually by delamination and by progressive pullout of the flexible roots (Figure 2).

A simplified model representative of the observed failure modes was established by considering that each root i develops a moment m_i with one component related to the root strength (m^i_{root}) and the other related to its interaction with the surrounding soil ($m^i_{root/soil}$). The total resisting moment results from the sum of the resistance of the N roots:

$$M(\alpha_r) = \sum_{i=1}^{N} m^i(\alpha_r) = \sum_{i=1}^{N} [m^i_{root}(\alpha_r) + m^i_{root/soil}(\alpha_r)]. \tag{3}$$

At failure, when the root system rotation α_r reaches the critical rotation α_r^c, the critical resisting moment can be written :

$$M_c = M_c^{root} + M_c^{root/soil}. \tag{4}$$

The root component M_c^{root} contributing to the critical resisting moment can be expressed as follows :

$$M_c^{root} = \sum_{i=1}^{N} l_i a_i \sigma^i_{root}, \tag{5}$$

where σ^i_{root} is the root strength, a^i is the section area of the root i and l_i the lever arm of the resulting force (Fig. 4). The contribution of both mode of resistance to the critical turning moment, either by root strength or soil-root friction, is expected to depend on root size. The rupture threshold is given by the weakest component either the root or the root-soil interface breaking first. For small structural roots, the failure threshold will be mostly given by the root strength (σ^i_{root}). On the contrary, large roots are more resistant so that failure will occur preferentially at the soil-root interface.

The root/soil interface component $M_c^{root/soil}$ can be expressed as follows:

$$M_c^{root/soil} = C_0 + \frac{1}{S}\sum_i l^i S^i \tau_f^i, \tag{6}$$

with τ_f^i the average soil shear strength. S^i is the external surface of the root i and S is the total external surface of the root system. The term C_0 is a constant factor introduced to consider the possible interaction between roots. The complete development of the resistance of each root requires the mobilization of a certain volume of soil surrounding the root corresponding to its zone of influence. The proximity of the roots of each other within the root system leads to arching effects within the soil between the roots, and may result in a positive or negative contribution depending on the root system architecture (root diameter, spacing, connectivity, etc.), reflecting by C_0. This architectural mechanism has been studied extensively for pile groups (Patra et al., 2010; Shanker et al., 2006; Vanitha et al., 2007; Shelke and Patra, 2008) in the geotechnical engineering field.

Influence of soil water content. The root/soil interface component $M_c^{root/soil}$ is expected to vary with the soil water content in relation to τ_f^i. According the mechanics of unsaturated soils (Fredlund et al., 1978; Gan et al., 1988; Guan et al., 2010), each τ_f^i can be decomposed in a frictional τ_φ^i and suction component τ_ψ^i:

$$\tau_f^i = \tau_\varphi^i + \tau_\psi^i. \tag{7}$$

Then the root/soil interaction component of the critical resisting moment becomes:

$$M_c^{root/soil} = C_0 + M_\varphi + M_\psi, \tag{8}$$

with $M_\varphi = \frac{1}{S}\sum_i l^i S^i \tau_\varphi$ and $M_\psi = \frac{1}{S}\sum_i l^i S^i \tau^i_\psi$. When compiling Eq. 5 and Eq. 8, the critical resisting moment can be expressed as:

$$M_c = \sum_{i=1}^{N} l_i a_i \sigma^i_{root} + C_0 + \frac{1}{S}\sum_i l^i S^i \tau_\varphi + \frac{1}{S}\sum_i l^i S^i \tau^i_\psi. \tag{9}$$

2.3. Sub-model used for the soil mechanical strength

A sub-model was required to describe the evolution of the soil shear strength with soil water content in sandy soils. For each soil layer, the soil shear strength was evaluated using a similar procedure as described in Veylon et al. (2015). As the soil fine content was low, effective cohesion was assumed equal to zero. Therefore, the shear strength of Eq. 6 was modeled with the following failure criterion (Oberg and Sallfors, 1997):

$$\tau_f = (\sigma_n + S_r\psi)\tan\varphi_p, \tag{10}$$

where σ_n is the mean net vertical stress applied within each soil layer, φ_p its peak friction angle (deg.) at saturation, S_r its saturation ratio S_r=w_n/w_{sat} with w_{sat}, the soil gravimetric water content at saturation and ψ its matric suction. Both terms $\sigma_n \tan\varphi_p$ and $S_r\psi\tan\varphi_p$ correspond respectively to the frictional component (τ_ϕ) and to the suction component (τ_ψ) of the shear strength (τ_f) according to Eq. 7. The frictional component mainly depends on the soil porosity and on the mean effective stress as detailed in the following paragraph and increases with soil water content. The suction component due to the development of capillarity forces between soil grains decreases with soil saturation ratio.

The peak friction angle φ_p in the frictional component was estimated for each soil layer to account for its dependency on both the soil porosity and the pressure. It is well known that φ_p depends on the sand state (Been et al., 1991; Bolton, 1986) and that φ_p is not constant under very low pressure ($<$ 20 kPa)

(Fukushima and Tatsuoka, 1984; Tatsuoka et al., 1986; Baker, 2004; Fannin et al., 2005; Chakraborty and Salgado, 2010; Rouse, 2018). This phenomenon is attributed to the effect of dilatancy and can be modeled with the relative dilatancy index I_R following the stress-dilatancy theory (Rowe and Taylor, 1962; De Josselin De Jong, 1976; Bolton, 1986). To account for these effects, φ_p was estimated as a function of both the mean effective pressure p' and the void ratio e with $p' = \sigma_n(1 + 2K_0)/3$, K_0 is the horizontal earth pressure at rest, approximated here by $K_0 = 1.15 - \sin\varphi_c$ (Llano-Serna et al., 2018). The relationship used for φ_p was:

$$\varphi_p = \varphi_c + A_\Psi I_R, \tag{11}$$

where φ_c and A_Ψ are two constant parameters. The term I_R depends on p' and e as follows:

$$I_R = I_D(Q - \ln p') - 1. \tag{12}$$

Here, the term Q depends on p' while I_D depends on e. Q is a parameter that depends on the intrinsic sand characteristics and was estimated by the relation proposed by Chakraborty and Salgado (2010) based on a large database of experimental results on clean sands:

$$Q = 7.1 + 0.75\ln p'. \tag{13}$$

I_D is the relative density of the soil defined:

$$I_D = \frac{e_{max} - e}{e_{max} - e_{min}}. \tag{14}$$

2.4. Simulating the tree resistance to overturning for different soil water conditions

The possible effect of soil wetting on the critical resisting moment M_c (Eq. 9) was examined by simulating two saturation scenarios.

The first scenario consists in increasing the water table level. Such a rise in the water table level may be caused by continuous rainfall during a certain period of time (e.g. during winter). The model assumes that the soil profile is separated into a saturated zone under the water table level ($S_r = 1$) and an upper unsaturated zone ($S_r < 1$). Three different values of water table level are considered $\mathcal{WT}$ = -0.1 m, -0.4 m and -0.6 m. Under the water table level, the soil is considered as saturated and above the water table level, the soil has a variable saturation degree S_r.

The second scenario corresponds to the downward progression of a saturation front level. This case may occur according to infiltration mechanism in case of heavy rain concentrated in time. The model used for this scenario is the Green-Apmt model (Green and Ampt, 1911) widely used in water resources research field (Chen and Young, 2006; Kale and Sahoo, 2011). This model assumes a homogeneous soil profile and an uniform distribution of the initial saturation ratio. A saturation front separates the soil profile into an upper saturated zone ($S_r = 1$) and a lower unsaturated zone where the saturation ratio of the soil stays at its initial value ($S_r < 1$). Despite its simplicity, the Green-Ampt model provides a reasonably accurate estimate of the infiltration front evolution which is sufficient for most of the field problems (Whisler and Bouwer, 1970; Gill, 1978; Dagan and Bresler, 1983; Govindaraju et al., 1992; Kargas and Kerkides, 2011). Three different values of saturation front level are considered $\mathcal{SF}$ = 0.0 m, -0.1 m and -0.4 m. Above the saturation front level, the soil is considered as saturated and bellow the saturation front level, the soil has a variable saturation degree S_r.

2.5. Main hypothesis for model parametrization

The parameters used for the root dimensions came from the root architecture measurement and those for the soil strength from soil mechanical tests and soil-water retention measurements (following section 2.6) . Then, the other unknown parameters, M_0 and l_i, were estimated by fitting the field data critical turning moment M_c-data with the expression proposed for the tree resistance to overturning (Eq. 9).

These parameters estimations were based on different hypothesis:

- σ^i_{root} was assumed not to depend on its diameter in agreement to Genet et al. (2005) for roots higher than 2 mm;
- a_i was assumed to be proportional to S_i with S_i estimated from SRL ($S = 1/SRL$). SRL-values were estimated from the 3D-root architecture by grouping the roots according to the sector and the type they belong to : winching shallow root (S_W), counter winching shallow root (S_{WC}) or tap roots (S_T). The contribution of sinker roots to M_c was neglected;
- the surrounding soil was decomposed in three layers corresponding to 0-10 cm, 10-40 cm and 40-60 cm depths. The variation in the organic carbon content with soil depth was neglected. The effect of the tree weight was also neglected. Then the critical shear strength parameters only depended on the ρ_d and w_n values of each layer as previously described (section 2.3);
- the shallow roots develop mainly between 10 and 40 cm depth (Fig. 3). Then the shear strengths surrounding the shallow roots were estimated in the middle of the 10-40 cm from the measurement of the shear strength τ_f^{10-40}. Similarly the measurement τ_f^{40-60} were used to estimate the soil shear strengths surrounding the tap roots.

According to these hypothesis and Eq. 9, the expression for the critical resisting moment M_c was as follows:

$$M_c = M_0 + M_k^{10-40} + M_T^{40-60}, \quad (15)$$

with

$$M_k^{10-40} = \frac{S_k}{S}(l_k^{\varphi}\tau_{\varphi}^{10-40} + l_k^{\psi}\tau_{\psi}^{10-40}), \quad (16)$$

$$M_T^{60-40} = \frac{S_T}{S}(l_T^{\varphi}\tau_{\varphi}^{40-60} + l_T^{\psi}\tau_{\psi}^{40-60}), \quad (17)$$

where k=W or WC. M_0 is a constant with M_0= $C_0 + \sum_{i=1}^{N} l_i a_i \sigma_{root}^i$. l_W^{ψ}, l_{WC}^{φ}, l_{WC}^{ψ}, l_T^{φ}, l_T^{ψ} are constant parameters representing equivalent lever arms. These parameters are expected to be of the order of meters and can be positive or negative as they have favourable or unfavorable effect on the resisting moment. The lever arms coefficients l_i and M_0 were determined by multi-linear regression of the field M_c-data.

Once the parameters were estimated, the critical resisting moment M_c was calculated from Eq. 15 for both scenarios for which we considered a tree with the average characteristics (SRL, S_W, S_{WC} and S_T) measured for the 12 trees (Table 1).

2.6. Model parameters for the soil sub-model

For both simulated scenarios, the soil shear strengths for 10-40 and 40-60 and their variation with the soil layer water content were estimated from Eq. 10 for a range of saturation ratio between 0.1 to 1.

Net vertical stress σ_n. The net vertical stress σ_n was estimated at the middle of each layer, i.e. at 25 cm and 50 cm depths. We assumed that the weight of the tree can be neglected as regards to the vertical pressure induced by the soil overlying layers. Therefore, the net vertical stress only depends on the soil porosity and water contents of the soil overlying layers.

Matric suction ψ. Matric suction ψ were deduced from the water retention curve $S_r(\psi)$, estimated from soil-water retention measurements by considering a unique matric suction curve for both soil layers (10-40 or 40-60).

The water retention curve was determined using pressure plate method (Richards, 1941) from soil samples collected in the field site at 0-10, 10-40 and 40-60 cm. The pressure plate device consists of a pressure vessel which can be pressurised up to a air pressure of 1500 kPa. Soil samples were placed on a ceramic disc that has a specified air entry pressure value. The disc was connected to the atmosphere and water is allowed to flow out freely. Pressure steps were applied by a flow control valve and controlled by a pressure gauge. During the whole test, the temperature in laboratory was controlled at around 20 ^oC. In order to determine the balance time under each pressure, the samples were removed and weighted using electronic scales having accuracy of 0.01 g every 12 h for each pressure step. If the mass of the sample remained unchanged after 24 h, then it was assumed to be in a state of equilibrium and the gravimetric water content was measured.

Samples per soil horizon were packed at ρ_d= 1.23, 1.41, 1.58 Mgm^{-3} for respectively soil layers 0-10, 10-40 and 40-60 cm in cylinder of 3.4 mm diameter and 1.9 mm height. These ρ_d-values corresponded those of the field pulling tests. Five air pressures were applied to three samples per soil horizon corresponding to matric suction equal to 1, 3.2, 10, 32 and 100 kPa.

The matric suction ψ was estimated from the saturation ratio S_r by modeling the soil-water retention curve-data (Fig.5). Over the years, a number of water retention curves have been proposed (Fredlund and Xing, 1994). The best fit to our experimental data was obtained using the model developed by Lebeau and

Konrad (2010) and validated by Konrad and Lebeau (2015). This model is not purely empirical but explicitly accounts for the mechanisms of water retention (capillarity and adsorption):

$$S_r = S_{rc} + (1 - S_{rc})S_{ra}, \tag{18}$$

with

$$S_{rc} = \begin{cases} 1 & \psi \leq \psi_a, \\ 1 - (1 - e^{-\Lambda\psi})^{\zeta} & \psi > \psi_a, \end{cases}$$

and

$$S_{ra} = S_{ro}\left(1 - \frac{\ln \psi}{\ln \psi_d}.\right)$$

In this expression, S_{rc} describes the effect of the capillary forces and S_{ra} the effect of the adsorptive forces. The parameters ζ and Λ are shape and scale parameters of the pore-size distribution, respectively. $\psi_a = \psi_d^{1-1/S_{ro}}$ is the matric suction for which the degree of saturation due to adsorption reaches 1, S_{ro} is the degree of saturation due to adsorption at a matric suction of 1 kPa and ψ_d is the matric suction at oven dryness, which is approximately 10^6 kPa. The parameters of the soil-water retention curve (Eq. 18) were determined by minimizing the square error between the calculated and measured saturation ratios. They were found equal to $S_{ro} = 0.11$, $\zeta = 0.62$ and Λ=0.49 ($R^2 = 0.86$). The adjusted water retention curve is represented on Fig.5.

To estimate the matric suction ψ, an approximation for the expression Eq. 18 was used in the range $S_r = 0.1 - 1.0$ where the capillary component is predominant:

$$\psi = -\frac{1.30}{\Lambda} \ln\left(1 - (1 - S_r)^{1/\zeta}\right). \tag{19}$$

Eq. 19 was used to estimate ψ as function of S_r in the expression used to evaluate soil shear strength (Eq. 10).

Peak friction angle φ_p. The peak friction angle φ_p was estimated for each soil layer (10-40 or 40-60) using direct shear tests. These laboratory tests were performed for both layers 10-40 and 40-60 for soil samples at different initial void ratio e, different net vertical stress σ_n and different saturation ratio S_r. Combined with the $S_r(\psi)$ curve, these tests allowed for estimating φ_c and A_ψ of the peak friction angle φ_p (Eqs.11-14).

Direct shear tests were conducted using a Wykeham Farrance shear testing machine to characterize the soil mechanical properties. Soil samples were collected at two horizons 10-40 and 40-60 cm depth in the field site. Soils were air dried and sieved through $<$2 mm. Soil samples were packed at two porosity corresponding to the dry bulk density ρ_d of 1.41 and 1.58 Mg m^{-3} of the soil of layers 10-40 and 40-60 cm for the 12 pulled tree locations. Four initial gravimetric water contents were tested: $w_n = 0.1$, 0.15, 0.2 and soil saturation. For unsaturated soil samples (w_n=0.1 to 0.2), soils were obtained by spraying dried sieved soils with water until the desired water content was reached, and then the specimens were compacted in cylinder at the desired initial bulk density. For saturated conditions, specimens were first packed in cylinders with soil at w_n=0.1 to obtain the initial desired bulk density. After sample preparation, the specimens were kept in airtight containers at 4^oC for at least 24 hours before being sheared (Oloo and Fredlund 1996). This duration was considered sufficient to ensure the equilibrium of air and water in the specimens (Wen and Yan, 2014). Then, the specimens were saturated directly in the shear cell following the procedure ASTM D 3080-90. The lateral displacement rate was 0.38 mm/min compatible with drained conditions. Each direct shear test provided one soil response curve relating the shear stress (τ) to the lateral relative displacement (δ) for four net vertical stress $\sigma_n = 3.17$, 6.01, 8.05 and 13.56 kPa.

The constant parameters φ_c and A_Ψ of the peak friction angle φ_p (Eqs.11-

14) were estimated from the φ_f-data. The stress-displacement response of each soil sample was analyzed individually to determine the pertinent values of shear strength (τ_f). The shear strength was determined as the maximum value of shear stress measured during the shear loading. When no peak value or plateau was observed, the test was rejected. The results for tests in saturated conditions are presented in Table 4. The values of φ_c and A_Ψ were determined by minimizing the square error between the τ_f-data measured for 10-40 and 40-60 and the calculation of τ_f obtained using Eq. 10 with σ_n the vertical stress applied during the direct shear tests and ψ the value calculated with Eq. 19 from the saturation ratio of the soil sample.

3. Results

3.1. Variations in the field the critical moment with soil water content

The overturning moment M is presented for the 12 trees in Fig.6 according to the rotation of the root-soil system α_r. The response curves M(α_r) exhibited typical elasto-plastic material behavior with a linear part at small angle and a transition to elasto-plastic range. The curve reached a maximum M_c that can be considered as the ultimate rupture of the soil-root system. The decrease in resisting moment was due to root breakages and pullout: the lateral roots were stretched and failed one after the other both in the counter winchward and in the winch ward side, the taproot failed by flexion or delamination (pictures not shown). Few M(α_r) curves exhibited oscillations during pulling, probably due to successive failures as the root slided (Fig. 6).

The tree anchorage resistance varied from 7.92 to 16.10 kN.m between the 12 trees (Table 2). Similarly the root-soil stiffness k_r varied among specimens between 1.69 and 3.91$\dot{\text{k}}$N$\dot{\text{m}}/^o$. M_c was positively and linearly correlated to k_r

with M_c= $0.24k_r$ (R^2=0.69, P<0.001), showing that the most flexible root-system had the lowest rupture strength.

The soil water conditions for tree pulling were different in the two series. The mean soil water contents were 0.13 and 0.24 g.g^{-1} for the first and the second series respectively and were significantly different using student-tests(Table 2). Note that this last value corresponds to measurements for only 2 depths (5, 20 cm) because of soil saturation at higher depth. In terms of soil saturation, the saturation ratio of the three soil layers in the first series ranged from S_r=0.098 to 0.182 whereas the minimum of S_r was 0.152 and all the 40-60 layers reached saturation ($S_r \approx 1$) in the second series.

Significant correlation was found between M_c-values and variables describing the root architecture, in particular R=0.88 (P<0.001) with the total volume of roots and R=-0.85 (P<0.001) with the total SRL (Table 3). On the contrary, the variations in ρ_d and w_n between trees and between series did not explain the M_c variations as no statistical correlation was found with these factors.

3.2. Estimation of soil shear strength using the soil sub-model

The shear strength τ_f deduced from the soil sub-model (Eq. 10) are compared to the measurements in Fig.8. τ_f-calculation are based on the constant parameters φ_c and A_Ψ of the peak friction angle φ_p (Eqs.11-14). The optimal value for φ_c was $\varphi_c = 34^o$, which is coherent with the nature of the soil (Sadrekarimi and Olson, 2011). The optimal value A_Ψ=3.7 was obtained and lies in the interval 3-5 of the admissible values (Bolton, 1986).

The correlation between τ_f-calculation and τ_f-measurement is $R^2 = 0.80$ and the predictive model error is less than 2 kPa, which is acceptable as regards to the expected in situ variability of soil properties, in particular the retention curve (Zapata et al., 2000) (Fig. 5). This illustrates the ability of the soil sub-model to predict with a reasonable accuracy the shear strength of the unsaturated soils interacting with the tree root systems.

3.3. Modelling the critical moment

The parameters of the M_c-model (Eq. 15) as estimated by multi-linear regression analysis of the M_c-data for the 12 tree specimen are presented in Table 5. The parameters l_i^j can be viewed as equivalent lever arms and reflect the contributions of the soil-root interactions to the resisting moment in each root sector. Their values are positive for all sectors (from 1.12 to 9.69 m) reflecting a favorable effect of the soil on the resisting moment, except for the roots in the counter winch sector where the value is -0.32 for the frictional component l_{wc}^{φ}. The comparison between the measured resisting moment and the resisting moment predicted by the model (Fig. 9) show that the predictive capacity of the model is fairly good (R^2=0.90 and SE=0.8 kN.m). The maximum relative error remains below 10% of the measured resisting moment which is low in comparison to the field variability measured for the root systems and for the soil layers(Tables 1 and 2).

3.4. Simulations of the tree resistance with soil saturation

Increase of the water table level. The first scenario simulates an increasing water table level $\mathcal{WT}$ from -0.6 m to -0.1 m. The evolution of the critical turning moment with the saturation ratio above the water table level is presented in Figure 10. It represents how M_c changes with the progressive wetting of the top soil horizon until the complete saturation of all the soil layers. For all water table levels, the critical turning moment slightly increases with saturation ratio. In the quasi-saturated domain, which is assumed to be reached for $S_r \geq 0.95$ (Monnet and Boutonnier, 2012), the curves abruptly collapse as the medium becomes quasi-completely saturated because the interstitial water porous network merges and the water can transmit pressure within the whole fluid phase.

Progression of a saturation front. In the second scenario, the rainfall induced a downward progression of a saturation front level ($\mathcal{SF}$). The evolution of the critical turning moment with the saturation ratio above the water table level is presented in Figure 11. It simulates how M_c changes as the lower layer wetting until full saturation. For all saturation front levels and S_r less than 0.20, the critical turning moment increases as the saturation ratio increases. Then, for higher values of saturation ratio and $\mathcal{SF}$ = 0.0 m and -0.4 m, M_c slightly deceases with saturation ratio. In the quasi-saturated domain ($S_r \geq$ 0.95), the same phenomenon occurs than for previous simulations : the curves abruptly collapse as the medium becomes quasi-completely saturated. For a given saturation ratio of the soil below the saturation front, M_c decreases as the saturation front progresses with depth. The evolution of the critical turning moment is quite limited when the saturation front progresses from 0.0 m et -0.1 m : M_c decreases by less than 1 kN.m for saturation ratios arround 0.2-0.25. As the saturation front progresses to -0.4 m, M_c decreases as the saturation ratio increases, but the diminution does not exceed 1 kN.m.

4. Discussion

Model parametrization and evaluation. The new model proposed here for tree anchorage improves the description of the mechanical processes in play at the root-soil interface and their variation with soil saturation. This model contains a sub-model for the soil shear properties. This soil sub-model for sandy soils accounts for the matric suction and also considers the packing soil state through p' and e. These last two variables have been recognized key in the strength of sandy soils at low pressure (Houlsby, 1991). The anchorage model also contains a description of root system through the distribution of the root surfaces per wind sector and per soil layers. In comparison, previous numerical studies have used a rough estimation of the soil mechanical properties with idealized soil types (Dupuy et al., 2005; Fourcaud et al., 2007) or parameters measured at high vertical pressure (Yang et al., 2014; Rahardjo et al., 2017, 2009, 2017; Yang et al., 2018). When the soil hydrology was considered, the authors used idealized root systems unrepresentative of the studied tree species (Rahardjo et al., 2009, 2017).

The present model was not designed to predict the risk of overturning but rather to analyze the mechanics of the root-soil system. Indeed the size of the test population (12) was small in relation to the number of regression variables: 7 parameters to be estimated. The justification for the choice of regression variables was based on mechanical considerations. In order to evaluate the sensitivity of the regression results, we performed "leave-one-out" cross validations on each test (Sammut C., 2010). We obtained 12 sets of regression coefficients calibrated on 11 tests leaving one test out for validation. The values of the mean and the standard error of regression coefficients obtained by the leave-one-out procedure did not exhibit large discrepancy with the parameters-values (Table 5). This cross validation procedure illustrates the relative robustness of the developed methodology and the degree of confidence that can be placed in simulations.

The developed methodology also appears corroborated by the parameters-values themselves. The values of the lever arms are in the order of a meter, which is consistent with the size of the root systems (Table1). The positive values traduce the favorable contributions of the soil-root interfaces to the resisting moment. The negative contribution obtained for the roots of the plate in the counter winch sector could be interpreted as the effect of deconfinement of the soil under roots located in the counter winch sector as the root system rotates. In this sector, the roots tend to pull out during uprooting (Fig.2) thus reducing the resistance to overturning by the root-soil complex. The more roots in this sector, the more soil deconfinement occurs.

This model is also consistent with the data of Kamimura et al. (2012) who performed tree-pulling experiments on 30 years old hinoki trees (DBH about 19 cm, $H = 16$ m) on a yellowish brown forest soil and an Andisol soil. Starting from the assumption that heavy rains during a typhoon decreases soil strength, Kamimura et al. (2012) investigated the effect of irrigation treatments on the tree stability. Kamimura et al. (2012) showed that the water content inside the soil-root plate tended to increase the tree stability. This can be interpreted by the increase of the load of the soil-root plate which corresponds in our model to the frictional component $\sigma_n \tan \varphi_p$ (Eq. 10). This last term depends on the above soil layer weight that increases with soil water content. Kamimura et al. (2012) found that the tree stability decreases with the water content below the root-soil plate. This observation is also coherent with the suction component $S_r \psi \tan \varphi_p$ of the model (Eq. 10) that increases when saturation ratio decreases with the capillarity forces between soil grains.

Understanding tree resistance to overturning as function of soil water content in a sandy soil. Our main focus was to investigate the assumption that water wetting decreases the anchorage strength by decreasing soil mechanical strength. Our finding suggest that this assessment is mitigated for sandy soils outside the full saturation conditions.

This is illustrated by our field experiment where M_c did not exhibit change with soil water wetting in the case of unsaturated soil conditions. These unsaturated soil conditions are representative of the soil conditions during windstorm in the Landes de Gascogne Forest. Until now, complete soil saturation remain rare in this area. This was evidenced by Deirmendjian et al. (2018) who reported that complete soil saturation was reached only two days over the period

2014-2015 for a young Maritime pine forest similar to the site studied here. But fully soil saturation conditions are expected to be more frequent with ongoing climate change because of the increase in the precipitation during winter when storms usually occur in Europe (Stocker et al., 2014; Gardiner et al., 2010).

Our simulations also departs from the assumption that soil rainfall-induced wetting decreases soil shear mechanical properties and thus the tree root resistance against wind storms. To date, calculations for clay soils showed that M_c was systematically lower in wetter soils (Rahardjo et al., 2009, 2017). Our simulations evidence for specificities of sandy soils.

In sandy soils, the evolution of the resisting moment with saturation ratio is nor monotonous and nor trivial. It depends on the distribution of the water within the tree anchoring mass. The water table level has a major influence on the evolution of the resisting moment for saturation ratio outside the quasi-saturated domain. It has an influence on the resisting moment in dry condition (above the water table level) and on the shape of the $S_r - M_c$ curve. Our analysis suggests that a sharp decrease in overturning resisting moment with the soil water content is susceptible to occur when parts of the anchoring mass of the root system reaches the quasi-saturated domain, for example when an intense rain episode occurs during a storm.

Our model allows for analyzing the different mechanical processes in play with soil wetting. Figure 12 shows the evolution of the different components of the resisting moment with the saturation ratio for a water table level $\mathcal{WT}$ = -0.40 m. The component (M_0) provides the most important part of the resistance to overturning (around 65%) and does not depend on the saturation state of the soil. It represents the resistance due to each individual root (σ^i_{root}) and the global effect of root system architecture (C_0). The frictional component (M_φ) represents a shear of the order of 30% increases as the saturation ratio increases. This phenomenon is due to the soil weight increase with soil water that increases the vertical stress applying to the soil-roots interface. The suction component (M_ψ) is negative and slightly decreases (less than 10%) the moment of resistance in the unsaturated domain. This can be explained by the saturation of the 40-60 cm layer and the existence of the corresponding hydrostatic pressure which level off the saturated soil layer. When the quasi-saturated domain is reached, the hydrostatic pressure is established throughout the whole soil mass and the hydrostatic pressure experiences a sudden drop of the order of 5 kPa corresponding to a hydrostatic charge of 0.5 m of water.

Implications for wind risk models. This study highlights the need to focus on the occurrence of saturation situations with high precipitations or floods to prevent wind risk for forest growing in sandy soils. More particularly, our observation on one sandy soil can be applied to the Landes de Gascogne Forest since the region has very low soil variability. The Landes de Gascogne Forest grows on podzols. The variation in texture of these soils is low and their spatial heterogeneity principally comes from the river network that induces the presence or absence of cemented horizon between 1 to 0.3 m depth corresponding to the fluctuation of the water table between winter and summer (Jolivet et al., 2007). For a perspective of preventing wind risk at regional scale, identifying and mapping the inundated areas to improve their drainage, is a first way of improvement. A second way would be to include the evolution of soil saturation in the wind risk models applied to the Landes de Gascogne Forest (Cucchi et al., 2005; Kamimura et al., 2016).

This study also provides observations useful for wind risk models. The overturning stiffness of the root system k_{root} was found to be highly linearly correlated to M_c. Such a correlation is one of the first observation for forest trees (Sagi et al., 2019). From a practical point of view, measurements of k_{root} instead of M_c could be an alternative method to avoid systematic tree damage when performing tree winching tests. Until now, wind risk models are based on numerous destructive tree pulling tests on different species and different soil conditions for estimating the anchorage resistance. This finding suggests systematically measuring k_{root} when pulling tests to establish robust relationships $M_c(k_{root})$ for different species and soils.

5. Conclusion

This study presents new insights into the soil water content influence on tree anchorage. A new model for tree anchorage was developed involving an accurate description of the soil mechanical properties and the architecture of roots. This model is generic and could be transferable to trees of various developmental stages, different species and different soils in future studies. Combined with field-data, model simulations suggest that the anchorage of young *Pinus Pinaster* in sandy soil does not decrease drastically with soil wetting until the soil reach full saturation. This finding departs from previous findings. We argue that the difference is primary due to the specificity of sandy soils. Our analysis show that complete soil saturation in sandy soil induces a considerable drop in the tree anchorage. This result could have important implication for wind risk in forests growing in sandy soils in Europe. With climate change, storms will occur with heavier rainfall leading to more saturated soils inducing a higher risk of wind damage.

Acknowledgments

The authors would like to acknowledge Dr. Sylvain Dupont for his critical readings of the manuscript. This work was financially supported by the

Aquitaine Region with the FAST-A project, and by the French National Research Agency (ANR) with the TWIST (ANR-13-JS06-0006) and FOR-WIND (ANR-12-AGRO-0007) projects. This study has been also carried out in the framework of the Cluster of Excellence COTE (ANR-10-LABX-45).

References

Baker, R., 2004. Nonlinear Mohr envelopes based on triaxial data. Journal of Geotechnical and Geoenvironmental Engineeringm 130, 498–506. doi:10.1061/(ASCE)1090-0241(2004)130:5(498).

Been, K., Jefferies, M.G., Hachey, J., 1991. The critical state of sands. Géotechnique 41, 365–381. doi:10.1680/geot.1991.41.3.365.

Bolton, M.D., 1986. The strength and dilatancy of sands. Géotechnique 36, 65–78. doi:10.1680/geot.1986.36.1.65.

Chakraborty, T., Salgado, R., 2010. Dilatancy and shear strength of sand at low confining pressures. Journal of Geotechnical and Geoenvironmental Engineering 136, 527–532. doi:10.1061/(ASCE)GT.1943-5606.0000237.

Chen, L., Young, M.H., 2006. Green-Ampt infiltration model for sloping surfaces. Water Resources Research 42. doi:10.1029/2005WR004468.

Coutts, M.P., 1986. Components of tree stability in sitka spruce on peaty gley soil. Forestry 59(2), 173–197. doi:10.1093/forestry/59.2.173.

Cubrinovski, M., Ishihara, K., 2002. Maximum and minimum void ratio characteristics of sands. Soils and Foundations 42, 65–78. doi:10.3208/sandf.42.6_65.

Cucchi, V., Meredieu, C., Stokes, A., de Coligny, F., Suarez, J., Gardiner, B.A., 2005. Modelling the windthrow risk for simulated forest stands of Maritime pine (Pinus pinaster Ait.). Forest Ecology and Management 213, 184–196. URL: http://linkinghub.elsevier.com/retrieve/pii/S0378112705002240, doi:10.1016/j.foreco.2005.03.019.

Dagan, G., Bresler, E., 1983. Unsaturated flow in spatially variable fields: 1. Derivation of models of infiltration and redistribution. Water Resources Research 19, 413–420. doi:10.1029/WR019i002p00413.

Danjon, F., Fourcaud, T., Bert, D., 2005. Root architecture and wind-firmness of mature Pinus pinaster. New Phytologist 168, 387–400. doi:10.1111/j.1469-8137.2005.01497.x.

Danquechin Dorval, A., Meredieu, C., Danjon, F., 2016. Anchorage failure of young trees in sandy soils is prevented by a rigid central part of the root system with various designs. Annals of Botany 118, 747–762. doi:10.1093/aob/mcw098.

De Josselin De Jong, G., 1976. Rowe's stress-dilatancy relation based on friction. Géotechnique 26, 527–534. doi:10.1680/geot.1976.26.3.527.

Deirmendjian, L., Loustau, D., Augusto, L., Lafont, S., Chipeaux, C., Poirier, D., Abril, G., 2018. Hydro-ecological controls on dissolved carbon dynamics in groundwater and export to streams in a temperate pine forest. Biogeosciences 15, 669–691. doi:10.5194/bg-15-669-2018.

Dupuy, L., Fourcaud, T., Stokes, A., 2005. A Numerical Investigation into the Influence of Soil Type and Root Architecture on Tree Anchorage. Plant and Soil 278, 119–134. doi:10.1007/s11104-005-7577-2.

Dupuy, L.X., Fourcaud, T., Lac, P., Stokes, A., 2007. A generic 3D finite element model of tree anchorage integrating soil mechanics and real root system architecture. American Journal of Botany 94, 1506–1514. doi:10.3732/ajb.94.9.1506.

Ennos, A.R., 2000. The mechanics of root anchorage, in: Advances in Botanical Research. Academic Press. volume 33, pp. 133–157. doi:10.1016/S0065-2296(00)33042-7.

Fan, C.C., Su, C.F., 2009. Effect of soil moisture content on the deformation behaviour of root-reinforced soils subjected to shear. Plant and Soil 324, 57–69. doi:10.1007/s11104-008-9856-1.

Fannin, R.J., Eliadorani, A., Wilkinson, J.M.T., 2005. Shear strength of cohesionless soils at low stress. Géotechnique 55, 467–478. doi:10.1680/geot.2005.55.6.467.

Fourcaud, T., Ji, J.N., Zhang, Z.Q., Stokes, A., 2007. Understanding the Impact of Root Morphology on Overturning Mechanisms: A Modelling Approach. Annals of Botany 101, 1267–1280. doi:10.1093/aob/mcm245.

Fredlund, D.G., Morgenstern, N.R., Widger, R.A., 1978. The shear strength of unsaturated soils. Canadian Geotechnical Journal 15, 313–321. doi:10.1139/t78-029.

Fredlund, D.G., Xing, A., 1994. Equations for the soil-water characteristic curve. Canadian Geotechnical Journal 31, 521–532. doi:10.1139/t94-061.

Fukushima, S., Tatsuoka, F., 1984. Strength and deformation characteristics of saturated sand at extremely low pressure. Soils and Foundations 24, 30–48.

Gan, J.K.M., Fredlund, D.G., Rahardjo, H., 1988. Determination of the shear strength parameters of an unsaturated soil using the direct shear test. Canadian Geotechnical Journal 25, 500–510. doi:10.1139/t88-055.

Gardiner, B., Berry, P., Moulia, B., 2016. Review: Wind impacts on plant growth, mechanics and damage. Plant Science 245, 94–118. doi:10.1016/j.plantsci.2016.01.006.

Gardiner, B., Blennow, K., Carnus, J.M., Fleischer, P., 2010. Destructive Storms in European Forests: Past and Forthcoming Impacts. Final Report to EC DG Environment. European Forest Institute. URL: `http://ec.europa.eu/environment/forests/fprotection.htm`.

Genet, M., Kokutse, N., Stokes, A., Fourcaud, T., Cai, X., Ji, J., Mickovski, S., 2008. Root reinforcement in plantations of Cryptomeria japonica D. Don: effect of tree age and stand structure on slope stability. Forest Ecology and Management 256, 1517 – 1526. doi:10.1016/j.foreco.2008.05.050.

Genet, M., Stokes, A., Fourcaud, T., Norris, J.E., 2010. The influence of plant diversity on slope stability in a moist evergreen deciduous forest. Ecological Engineering 36, 265 – 275. doi:10.1016/j.ecoleng.2009.05.018. special Issue: Vegetation and Slope Stability.

Genet, M., Stokes, A., Salin, F., Mickovski, S.B., Fourcaud, T., Dumail, J.F., van Beek, R., 2005. The Influence of Cellulose Content on Tensile Strength in Tree Roots. Plant and Soil 278, 1–9. URL: `https://doi.org/10.1007/s11104-005-8768-6`, doi:10.1007/s11104-005-8768-6.

Gill, M.A., 1978. A layered infiltration model for homogeneous soils. Journal of Hydrology 36, 121 – 131. doi:10.1016/0022-1694(78)90042-2.

Gonzalez-Ollauri, A., Mickovski, S.B., 2017. Plant-soil reinforcement response under different soil hydrological regimes. Geoderma 285, 141 – 150. doi:10.1016/j.geoderma.2016.10.002.

Govindaraju, R.S., Or, D., Kavvas, M.L., Rolston, D.E., Biggar, J., 1992. Error analyses of simplified unsaturated flow models under large uncertainty in hydraulic properties. Water Resources Research 28, 2913–2924. doi:10.1029/92WR01515.

Green, H.W., Ampt, G.A., 1911. Studies on Soil Phyics. The Journal of Agricultural Science 4, 1–24. doi:10.1017/S0021859600001441.

Guan, G.S., Rahardjo, H., Choon, L.E., 2010. Shear strength equations for unsaturated soil under drying and wetting. Journal of Geotechnical and Geoenvironmental Engineering 136, 594–606. doi:10.1061/(ASCE)GT.1943-5606.0000261.

Hales, T.C., Miniat, C.F., 2017. Soil moisture causes dynamic adjustments to root reinforcement that reduce slope stability. Earth Surface Processes and Landforms 42, 803–813. doi:10.1002/esp.4039.

Houlsby, G.T., 1991. How the dilatancy of soils affects their behaviour, in: Presented at the 10th European Conference on Soil Mechanics and Foundation Engineering, University of Oxford. pp. 1–28.

Jolivet, C., Augusto, L., Trichet, P., Arrouays, D., 2007. Forest soils in the Gascony Landes Region: formation, history, properties and spatial variability. Revue Forestière Française LIX, 7–30. doi:10.4267/2042/8480.

Jonsson, M.J., Foetzki, A., Kalberer, M., Lundström, T., Ammann, W., Stöckli, V., 2006. Root-soil rotation stiffness of Norway spruce (Picea abies (L.)

Karst) growing on subalpine forested slopes. Plant and Soil 285, 267–277. doi:10.1007/s11104-006-9013-7.

Kale, R.V., Sahoo, B., 2011. Green-Ampt Infiltration Models for Varied Field Conditions: A Revisit. Water Resources Management 25, 3505. doi:10.1007/s11269-011-9868-0.

Kamimura, K., Gardiner, B., Dupont, S., Guyon, D., Meredieu, C., 2016. Mechanistic and statistical approaches to predicting wind damage to individual maritime pine (Pinus pinaster) trees in forests. Canadian Journal of Forest Research 46, 88–100. doi:10.1139/cjfr-2015-0237. wOS:000370049100009.

Kamimura, K., Kitagawa, K., Saito, S., Mizunaga, H., 2012. Root anchorage of hinoki (Chamaecyparis obtuse (Sieb. Et Zucc.) Endl.) under the combined loading of wind and rapidly supplied water on soil: analyses based on tree-pulling experiments. European Journal of Forest Research 131, 219–227. doi:10.1007/s10342-011-0508-2.

Kargas, G., Kerkides, P., 2011. A Contribution to the Study of the Phenomenon of Horizontal Infiltration. Water Resources Management 25, 1131–1141. doi:10.1007/s11269-010-9671-3.

Kim, J.H., Fourcaud, T., Jourdan, C., Maeght, J.L., Mao, Z., Metayer, J., Meylan, L., Pierret, A., Rapidel, B., Roupsard, O., de Rouw, A., Sanchez, M.V., Wang, Y., Stokes, A., 2017. Vegetation as a driver of temporal variations in slope stability: The impact of hydrological processes. Geophysical Research Letters 44, 4897–4907. doi:10.1002/2017GL073174.

Konrad, J.M., Lebeau, M., 2015. Capillary-based effective stress formulation for predicting shear strength of unsaturated soils. Canadian Geotechnical Journal 52, 2067–2076. doi:10.1139/cgj-2014-0300.

Lebeau, M., Konrad, J.M., 2010. A new capillary and thin film flow model for predicting the hydraulic conductivity of unsaturated porous media. Water Resources Research 46. doi:10.1029/2010WR009092.

Lindroth, A., Lagergren, F., Grelle, A., Klemedtsson, L., Langvall, O., Weslien, P., Tuulik, J., 2009. Storms can cause Europe-wide reduction in forest carbon sink. Global Change Biology 15, 346–355. URL: https://onlinelibrary.wiley.com/doi/abs/10.1111/j.1365-2486.2008.01719.x, doi:10.1111/j.1365-2486.2008.01719.x.

Llano-Serna, M.A., Farias, M.M., Pedroso, D.M., Williams, D.J., Sheng, D., 2018. An assessment of statistically based relationships between critical state parameters. Géotechnique 68, 556–560. doi:10.1680/jgeot.16.T.012.

Lundström, T., Jonsson, M.J., Kalberer, M., 2007. The root–soil system of Norway spruce subjected to turning moment: resistance as a function of rotation. Plant and Soil 300, 35–49. doi:10.1007/s11104-007-9386-2.

Monnet, J., Boutonnier, L., 2012. Calibration of an unsaturated air–water–soil model. Archives of Civil and Mechanical Engineering 12, 493–499. doi:10.1016/j.acme.2012.07.001.

Moore, J.R., 2000. Differences in maximum resistive bending moments of Pinus radiata trees grown on a range of soil types. Forest Ecology and Management 135, 63–71. doi:10.1016/S0378-1127(00)00298-X.

Neild, S.A., Wood, C.J., 1999. Estimating stem and root-anchorage flexibility in trees. Tree Physiology 19, 141–151. doi:10.1093/treephys/19.3.141.

Nicoll, B.C., Gardiner, B.A., Rayner, B., Peace, A.J., 2006. Anchorage of coniferous trees in relation to species, soil type, and rooting depth. Canadian Journal of Forest Research 36, 1871–1883. doi:10.1139/x06-072.

Oberg, A., Sallfors, G., 1997. Determination of Shear Strength Parameters of Unsaturated Silts and Sands Based on the Water Retention Curve. Geotechnical Testing Journal 20, 40–48. doi:10.1520/GTJ11419J.

Osman, N., Barakbah, S.S., 2006. Parameters to predict slope stability-Soil water and root profiles. Ecological Engineering 28, 90–95. URL: http://www.sciencedirect.com/science/article/pii/S0925857406000784, doi:10.1016/j.ecoleng.2006.04.004.

Patra, C., Sivakugan, N., Das, B., Rout, S., 2010. Correlations for relative density of clean sand with median grain size and compaction energy. International Journal of Geotechnical Engineering 4, 195–203. doi:10.3328/IJGE.2010.04.02.195-203.

Pollen, N., 2007. Temporal and spatial variability in root reinforcement of streambanks: Accounting for soil shear strength and moisture. CATENA 69, 197–205. doi:10.1016/j.catena.2006.05.004.

Rahardjo, H., Amalia, N., Choon, L.E., Harnas, F.R., Tieng, L.T., King, F.Y., 2017. Flux boundary measurements for the study of tree stability. Landscape and Ecological Engineering 13, 81–92. doi:10.1007/s11355-016-0303-9.

Rahardjo, H., Harnas, F.R., Leong, E.C., Tan, P.Y., Fong, Y.K., Sim, E.K., 2009. Tree stability in an improved soil to withstand wind loading. Urban Forestry & Urban Greening 8, 237–247. doi:10.1016/j.ufug.2009.07.001.

Rahardjo, H., Satyanaga, A., Leong, E.C., Santoso, V.A., Ng, Y.S., 2014. Performance of an instrumented slope covered with shrubs and deep-rooted grass. Soils and Foundations 54, 417 – 425. doi:10.1016/j.sandf.2014.04.010.

Richards, L.A., 1941. A pressure-membrane extraction apparatus for soil solution. Soil Science 51, 377–386.

Rouse, P.C., 2018. Relation between the critical state friction angle of sands and low vertical stresses in the direct shear test. Soils and Foundations 58, 1282 – 1287. doi:10.1016/j.sandf.2018.06.005.

Rowe, P.W., Taylor, G.I., 1962. The stress-dilatancy relation for static equilibrium of an assembly of particles in contact. Proceedings of the Royal Society of London. Series A. Mathematical and Physical Sciences 269, 500–527. doi:10.1098/rspa.1962.0193.

Sadrekarimi, A., Olson, S.M., 2011. Critical state friction angle of sands. Géotechnique 61, 771–783. doi:10.1680/geot.9.P.090.

Sagi, P., Newson, T., Miller, C., Mitchell, S., 2019. Stem and root system response of a Norway spruce tree (Picea abies L.) under static loading. Forestry: An International Journal of Forest Research 92, 460–472. URL: https://academic.oup.com/forestry/article/92/4/460/5524738, doi:10.1093/forestry/cpz042.

Sammut C., W.G.I., 2010. Leave-One-Out Cross-Validation, in: Sammut, C., Webb, G.I. (Eds.), Encyclopedia of Machine Learning. Springer US, Boston, MA, pp. 600–601. doi:10.1007/978-0-387-30164-8_469.

Schelhaas, M.J., 2008. The wind stability of different silvicultural systems for Douglas-fir in the Netherlands: a model-based approach. Forestry: An International Journal of Forest Research 81, 399–414. doi:10.1093/forestry/cpn028.

Schwarz, M., Cohen, D., Or, D., 2010. Root-soil mechanical interactions during pullout and failure of root bundles. Journal of Geophysical Research: Earth Surface 115, 1–19. doi:10.1029/2009JF001603.

Seidl, R., Schelhaas, M.J., Rammer, W., Verkerk, P.J., 2014. Increasing forest disturbances in Europe and their impact on carbon storage. Nature Climate Change 4, 806–810. doi:10.1038/nclimate2318.

Shanker, K., Basudhar, P.K., Patra, N.R., 2006. Uplift capacity of pile groups embedded in sands: predictions and performance. Soils and Foundations 46, 605–612. doi:10.3208/sandf.46.605.

Shelke, A., Patra, N.R., 2008. Effect of Arching on Uplift Capacity of Pile Groups in Sand. International Journal of Geomechanics 8, 347–354. doi:10.1061/(ASCE)1532-3641(2008)8:6(347).

Simon, A., Collison, A.J.C., 2002. Quantifying the mechanical and hydrologic effects of riparian vegetation on streambank stability. Earth Surface Processes and Landforms 27, 527–546. doi:10.1002/esp.325.

Stocker, T.F., Qin, D., Plattner, G.K., Tignor, M.M.B., Allen, S.K., Boschung, J., Nauels, A., Xia, Y., Bex, V., Midgley, P.M. (Eds.), 2014. Climate Change 2013: The Physical Science Basis. Cambridge Univ Press, Cambridge, United Kingdom and New York, NY, USA. doi:10.1017/CBO9781107415324.

Stokes, A., Norris, J.E., van Beek, L.P.H., Bogaard, T., Cammeraat, E., Mickovski, S.B., Jenner, A., Di Iorio, A., Fourcaud, T., 2008. How Vegetation Reinforces Soil on Slopes, in: Norris, J.E., Stokes, A., Mickovski, S.B., Cammeraat, E., van Beek, R., Nicoll, B.C., Achim, A. (Eds.), Slope Stability and Erosion Control: Ecotechnological Solutions. Springer Netherlands, Dordrecht, pp. 65–118. doi:10.1007/978-1-4020-6676-4_4.

Tatsuoka, F., Sakamoto, M., Kawamura, T., Fukushima, S., 1986. Strength and deformation characteristics of sand in plane strain compression at extremely low pressure. Soils and Foundations 26, 65–84. doi:10.3208/sandf1972.26.65.

Vanitha, L., Patra, N.R., Chandra, S., 2007. Uplift capacity of pile group anchors. Geotechnical and Geological Engineering 25, 339–347. doi:10.1007/s10706-006-9114-3.

Veylon, G., Ghestem, M., Stokes, A., Bernard, A., 2015. Quantification of mechanical and hydric components of soil reinforcement by plant roots. Canadian Geotechnical Journal 52, 1839–1849. doi:10.1139/cgj-2014-0090.

Wen, B.P., Yan, Y.J., 2014. Influence of structure on shear characteristics of the unsaturated loess in lanzhou, china. Engineering Geology 168, 46–58. doi:10.1016/j.enggeo.2013.10.023.

Whisler, F.D., Bouwer, H., 1970. Comparison of methods for calculating vertical drainage and infiltration for soils. Journal of Hydrology 10, 1 – 19. doi:10.1016/0022-1694(70)90051-X.

Wu, T.H., 2013. Root reinforcement of soil: review of analytical models, test results, and applications to design. Canadian Geotechnical Journal 50, 259–274. doi:10.1139/cgj-2012-0160.

Yang, K.H., Uzuoka, R., Thuo, J.N., Lin, G.L., Nakai, Y., 2017. Coupled hydro-mechanical analysis of two unstable unsaturated slopes subject to rainfall infiltration. Engineering Geology 216, 13–30. doi:10.1016/j.enggeo.2016.11.006.

Yang, M., Défossez, P., Danjon, F., Fourcaud, T., 2014. Tree stability under wind: simulating uprooting with root breakage using a finite element method. Annals of Botany 114, 695–709. doi:10.1093/aob/mcu122.

Yang, M., Défossez, P., Danjon, F., Fourcaud, T., 2018. Analyzing key factors of roots and soil contributing to tree anchorage of *Pinus* species. Trees 32, 703–712. doi:10.1007/s00468-018-1665-4.

Zapata, C.E., Houston, W.N., Houston, S., Walsh, K.D., 2000. Soil-water characteristic curve variability, in: Proceedings of Sessions of Geo-

Denver 2000 - Advances in Unsaturated Geotechnics, GSP 99, pp. 84–124. doi:10.1061/40510(287)7. sessions of Geo-Denver 2000 - Advances in Unsaturated Geotechnics, GSP 99 ; Conference date: 05-08-2000 Through 08-08-2000.

Trees	H	DBH	V_{root}	SRL	S_W	S_{CW}	S_T
11	10.12	0.1623	32786	0.70	1233.3	1151.3	1986.0
12	10.00	0.1814	41793	0.57	761.8	1537.8	1833.7
13	11.48	0.1751	40592	0.58	1807	3351.3	1375.2
31	9.70	0.1687	33234	0.78	1013.8	2049.8	1885.6
32	9.38	0.1687	25513	0.79	849.1	1372.4	1918.1
33	9.78	0.1783	35984	0.57	1780.6	875.0	1467.6
14	10.62	0.1798	34027	0.59	1412.7	1184.3	2158.7
15	10.40	0.1846	33336	0.52	1317.4	797.7	2853.5
16	11.15	0.1783	39816	0.57	1357.3	1446.2	2019.6
34	10.07	0.191	34673	0.58	140.9	1592.6	2196.3
35	11.65	0.1783	31520	0.53	319	2056.2	2140.2
36	10.65	0.1655	21775	1.15	2323	704.6	1607.4
Model	10.41	0.176	-	0.66	1193	1509.9	1953.5

H = Tree height (m), DBH = Stem diameter diameter at 1.3 m (m)
V_{root} = Root system volume, stump included (cm^3)
SRL = Specific Root Length, stump excluded $(cm.cm^{-3})$
S_W = root surface in the winching direction (cm^2)
S_{CW} = root surface in the counter winching direction (cm^2)
S_T = tap root surface (cm^2)

Table 1: Root architectural data of the 12 tree root systems after excavation and 3D digitizing and mean values used for simulations.

Test	11	12	13	31	32	33	14	15	16	34	35	36
k_r	3.52	3.63	3.70	3.10	2.25	3.91	3.36	3.01	3.11	3.61	3.56	1.69
M_c	14.33	14.73	16.10	12.78	10.61	14.10	15.07	13.94	14.88	12.12	13.68	7.92
α_r^c	8.1	10.0	13.8	13.7	12.9	13.2	13.7	15.4	10.5	8.0	8.8	18.0
Soil dry bulk density ρ_d (Mgm^{-3})												
0-10 cm	1.234	1.232	1.22	1.376	1.085	1.188	1.101	1.301	1.339	1.176	1.217	1.359
10-40 cm	1.596	1.52	1.348	1.333	1.373	1.281	1.49	1.225	1.616	1.453	1.42	1.256
40-60 cm	1.632	1.552	1.578	1.633	1.582	1.517						
Soil gravimetric water content w_n $(-)$												
0-10 cm	0.154	0.153	0.138	0.148	0.178	0.165	0.264	0.183	0.222	0.185	0.269	0.192
10-40 cm	0.063	0.072	0.112	0.132	0.135	0.107	0.213	0.267	0.206	0.245	0.288	0.307
40-60 cm	0.1	0.085	0.068	0.108	0.1	0.07	Sat	Sat	Sat	Sat	Sat	Sat
Saturation ratio S_r $(-)$												
0-10 cm	0.139	0.138	0.122	0.166	0.127	0.139	0.194	0.183	0.236	0.153	0.237	0.210
10-40 cm	0.100	0.101	0.121	0.139	0.151	0.104	0.286	0.238	0.338	0.310	0.347	0.287
40-60 cm	0.169	0.126	0.105	0.182	0.155	0.098	Sat	Sat	Sat	Sat	Sat	Sat

k_r = initial angular stiffness of the root system (kN.m/^{o}),
M_c = critical overturning moment (MN.m), α_r^c = critical angle (^{o})
w_n and ρ_d-values correspond to the average of four measurements

Table 2: Field data for the pulling tests under wet soil conditions in 2012 and very wet conditions in 2013.

M_c	
0.33	H
0.349	DBH
0.878****	V_{root}
-0.847****	SRL
-0.117	S_W
0.430	S_{CW}
0.070	S_T
0.002	ρ_d (0-10 cm)
-0.443	ρ_d (10-40 cm)
-0.247	ρ_d (40-60 cm)
-0.168	w_n (0-10 cm)
0.421	w_n (10-40 cm)
-0.101	w_n (40-60 cm)

Table 3: Correlation analysis for the critical turning moment with root architectural data and soil conditions.

Sample	e	w_n	S_r	σ_n	τ_f
Layer 10-40 cm					
L2-020-6	00.73	0.206	0.430	6.01	4.50
L2-020-8	0.71	0.199	0.416	8.05	7.46
L2-020-13	0.79	0.196	0.409	13.56	8.88
L2-015-3	0.84	0.167	0.349	3.17	3.08
L2-015-6	0.84	0.161	0.337	6.01	4.27
L2-015-8	0.84	0.167	0.348	8.05	5.57
L2-015-13	0.84	0.164	0.342	13.57	8.10
L2-010-3	0.84	0.109	0.228	3.17	3.00
L2-010-6	0.84	0.1	0.209	6.01	5.09
L2-010-8	0.84	0.106	0.221	8.05	5.21
L2-010-13	0.84	0.109	0.228	13.57	9.00
L2-sat-3	0.84	0.24	0.501	3.17	2.50
Layer 40-60 cm					
L3-020-3	0.65	0.188	0.755	3.17	4.52
L3-020-6	0.65	0.19	0.767	6.01	7.70
L3-020-8	0.65	0.211	0.848	8.05	8.04
L3-020-13	0.65	0.197	0.794	13.56	8.60
L3-015-3	0.65	0.127	0.512	3.17	5.45
L3-015-6	0.65	0.15	0.603	6.01	8.53
L3-015-8	0.65	0.181	0.73	8.04	9.30
L3-015-13	0.65	0.144	0.58	13.57	12.43
L3-010-3	0.65	0.094	0.38	3.17	4.50
L3-010-6	0.65	0.103	0.416	6.01	7.11
L3-010-8	0.65	0.101	0.405	8.05	7.70
L3-sat-3	0.69	0.258	0.973	3.17	4.80
L3-sat-6	0.69	0.263	0.993	6.01	4.80
L3-sat-8	0.69	0.256	0.965	8.05	6.80
L3-sat-13	0.69	0.259	0.979	13.57	9.60

e = void ratio (-), w_n = gravimetric water content (-), σ_n = vertical stress (kPa), τ_f

Table 4: The soil shear strength τ_f measured with the direct shear tests on the soil samples of layers 10-40 ċm and 40-60ċm corresponding to two void ratios e for different saturation ratio S_r and vertical stress σ_n. Each sample is designed by the layer (L2 or L3), the initial water content w_n from 0.10 to saturation and the vertical stress applied during tests from 3.17 to 13.57 kPa

	M_0	l_W^φ	l_{CW}^φ	l_T^φ	l_W^ψ	l_{WC}^ψ	l_T^ψ	R^2
Regression on all tests								
	8.40	3.28	-0.32	1.12	3.87	9.69	7.12	0.91
Regressions on tests by leaving one test out								
Mean	8.48	3.28	-0.23	1.10	3.67	9.01	6.99	0.89
S. Dev.	0.93	0.51	0.38	0.24	0.98	2.30	1.00	0.04

M_0 = constant factor (kN.m)

l_i^j = the lever arm coefficients (m)

Table 5: Parameters values obtained by multi-linear regression of the field critical turning moment data.

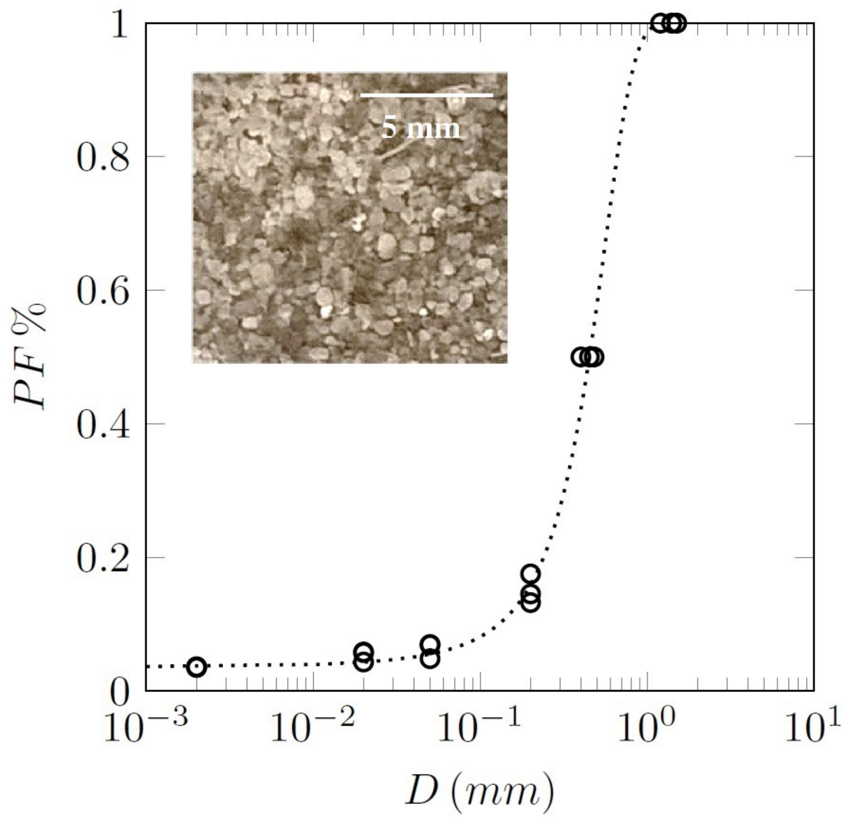

Figure 1: Particle size distribution of the substrate.

Figure 2: Root system after winching test. The zoom focus on the roots in the counterwinch sector that were pulled out the soil.

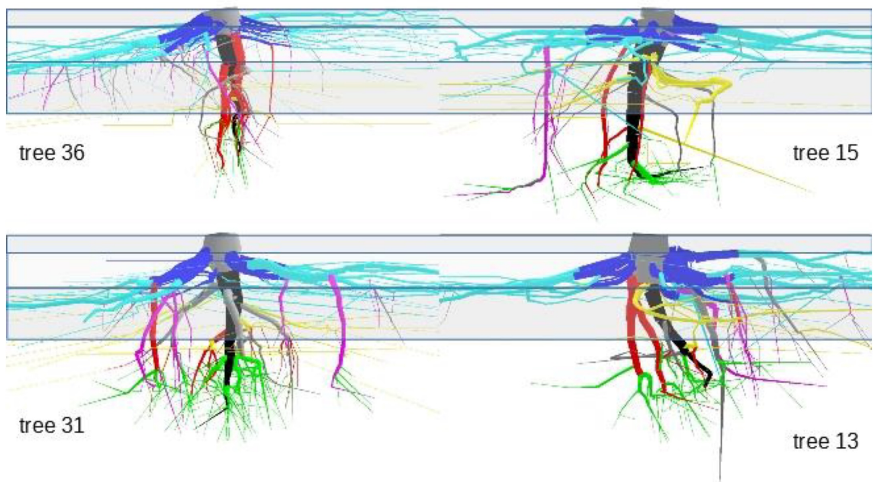

Figure 3: 3D reconstruction of four tree root systems. Segments were coloured according to their compartments according to Danquechin Dorval et al. (2016): (1) stump in grey, (2) taproot in black, (3) zone of rapid taper (ZRT) of horizontal shallow roots in dark blue, (4) horizontal shallow roots beyond the ZRT in light blue, (5) sinker roots branching from the ZRT in red, (6) sinker roots beyond the ZRT in magenta, (7) intermediate-depth horizontal roots in yellow, (8) deep roots in green, (9) oblique roots in dark grey. The 0-10, 10-30 and 30-60 depth soil layers are represented in shades of grey. The width of the whole figure is 5 m, with trees winched to the right. A reconstruction of root systems 34 and 35, perpendicular to the winching direction, can be found in Danquechin Dorval et al. (2016).

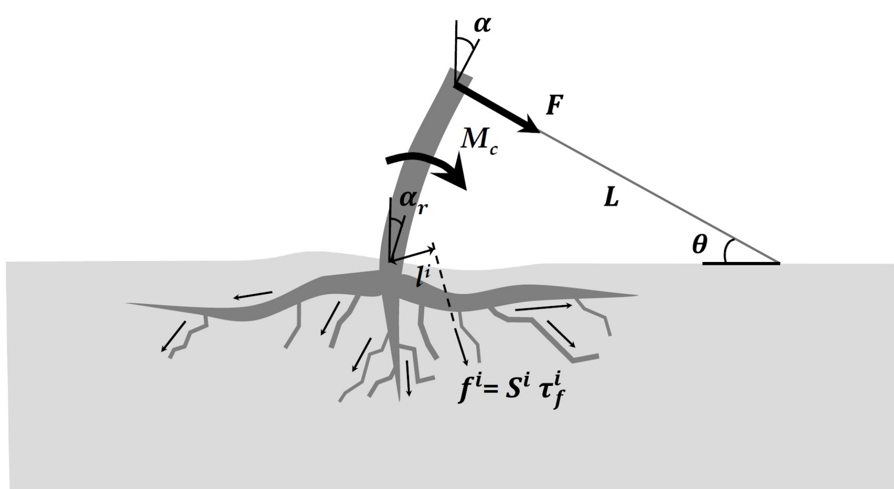

Figure 4: Mechanical model of the overturning root system. Each root i contributed to the critical resisting moment by it pullout resistance f^i and lever arm l^i.

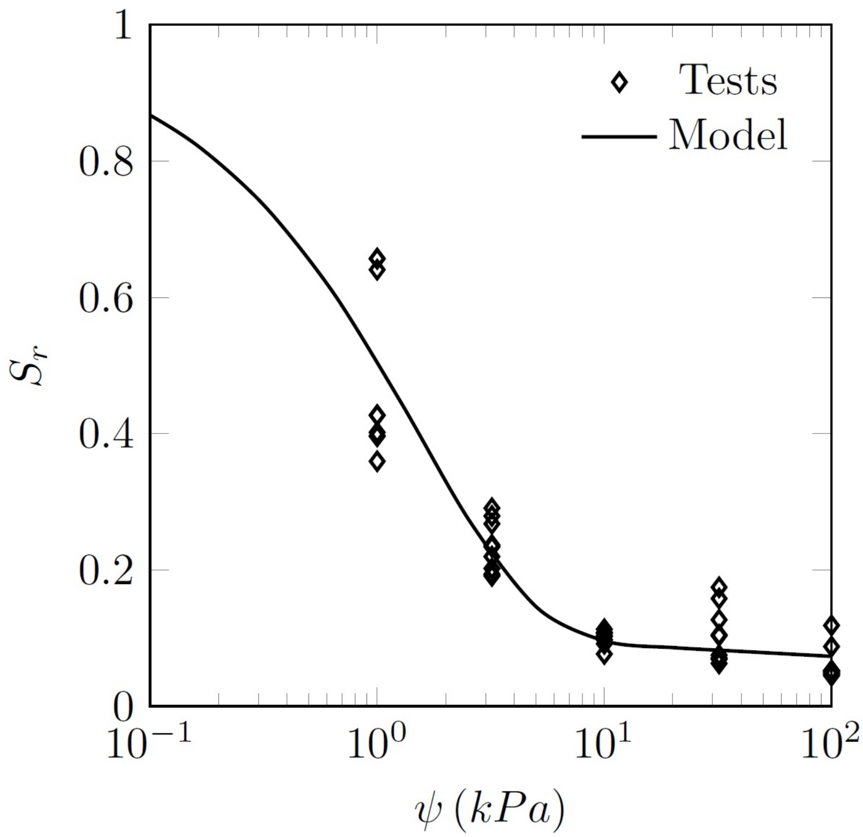

Figure 5: The water retention curve calibrated from the pressure plate tests for matric suction between 1 and 100 kPa.

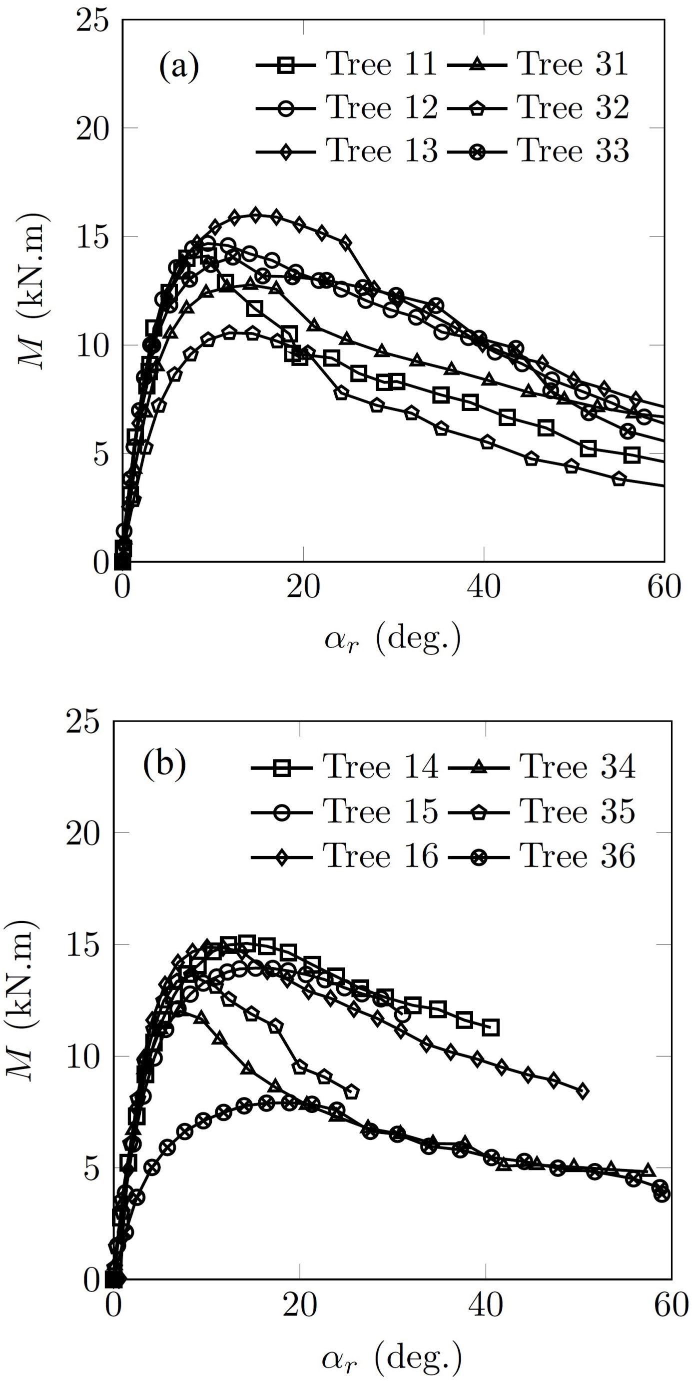

Figure 6: Response curves of turning moment measured for the 12 trees, 6 in 2012 (a) and 6 in 2013 (b) as function of the deflection angle at base of the tree α_r . The curves characterize a typical response of elasto-plastic material with a linear elastic part at small angle and a transition to plastic and damage part at higher angle. The maximum value of turning moment is considered as the ultimate rupture of the soil-root system and defines the critical bending moment M_c.

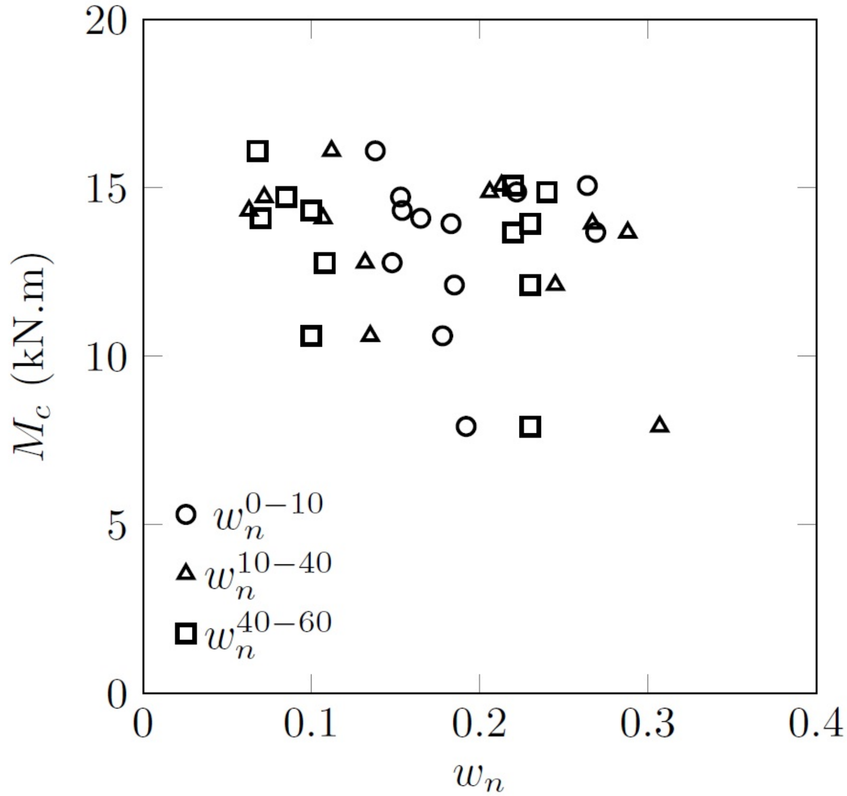

Figure 7: The critical turning moment M_c as a function of soil water contents representative of the three soil layers 0-10 cm, 10-40 cm and 40-60 cm.

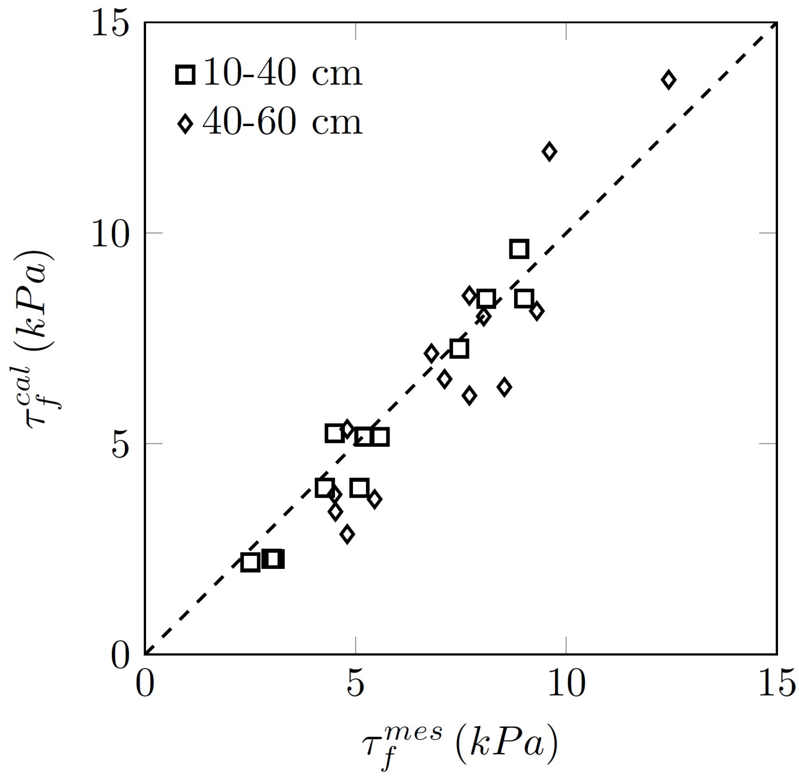

Figure 8: Comparison of the shear strength measured by direct shear tests (τ_{mes}) to the one calculated by the model (τ_{cal}). The determination coefficient is $R^2 = 0.80$.)

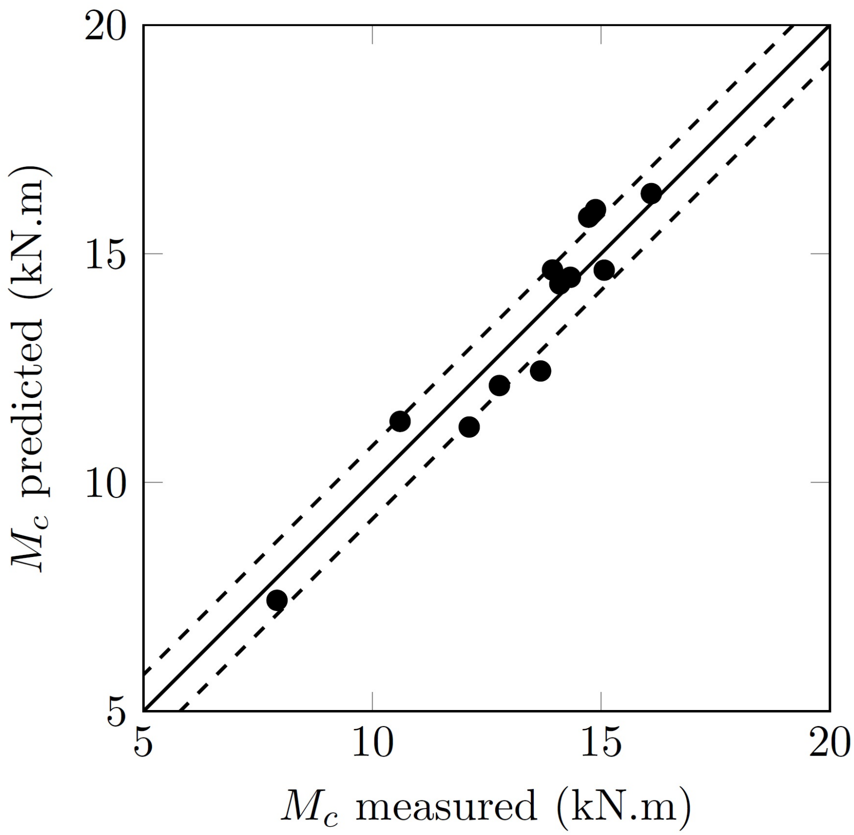

Figure 9: Representation of the critical turning moments measured during winching tests and predicted by the model (R^2=0.90). The dashed lines represent the regression line ± the standard error.

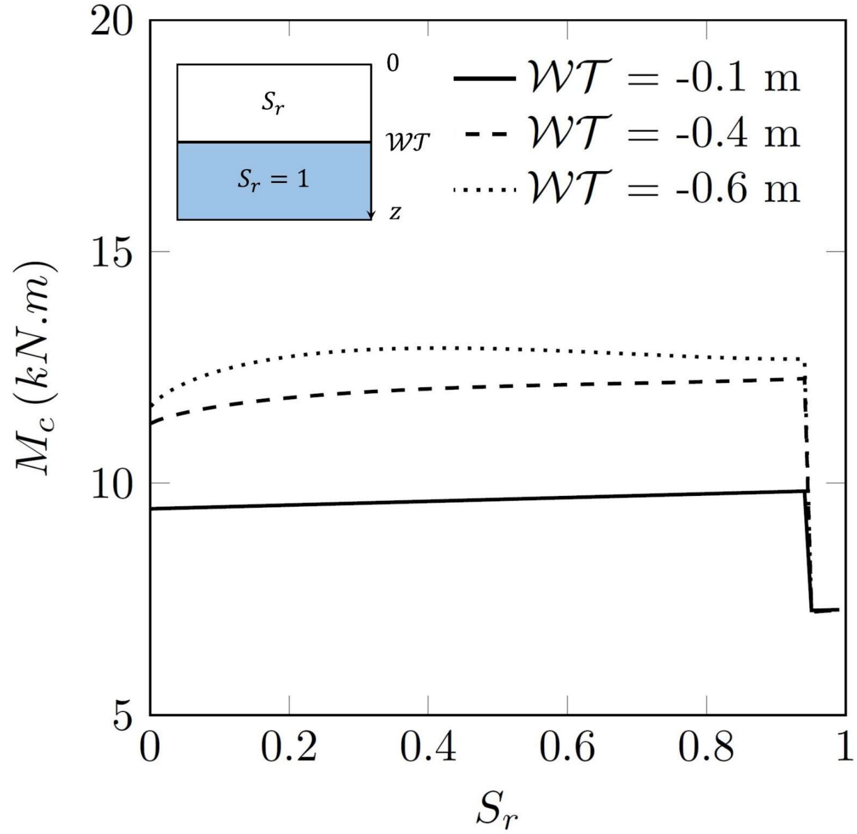

Figure 10: Representation of the critical turning moments predicted by the model as a function of water table level ($\mathcal{WT}$) and soil saturation ratio above the water table level.

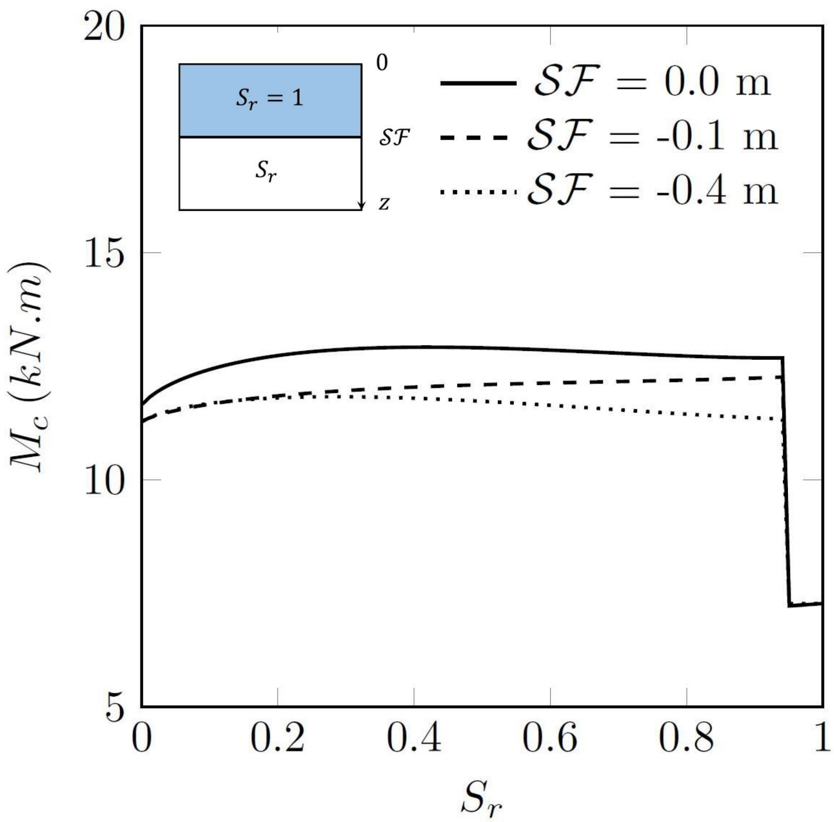

Figure 11: Simulation of the critical turning moment as a function of saturation front level ($\mathcal{SF}$) and soil saturation ratio below the saturation front.

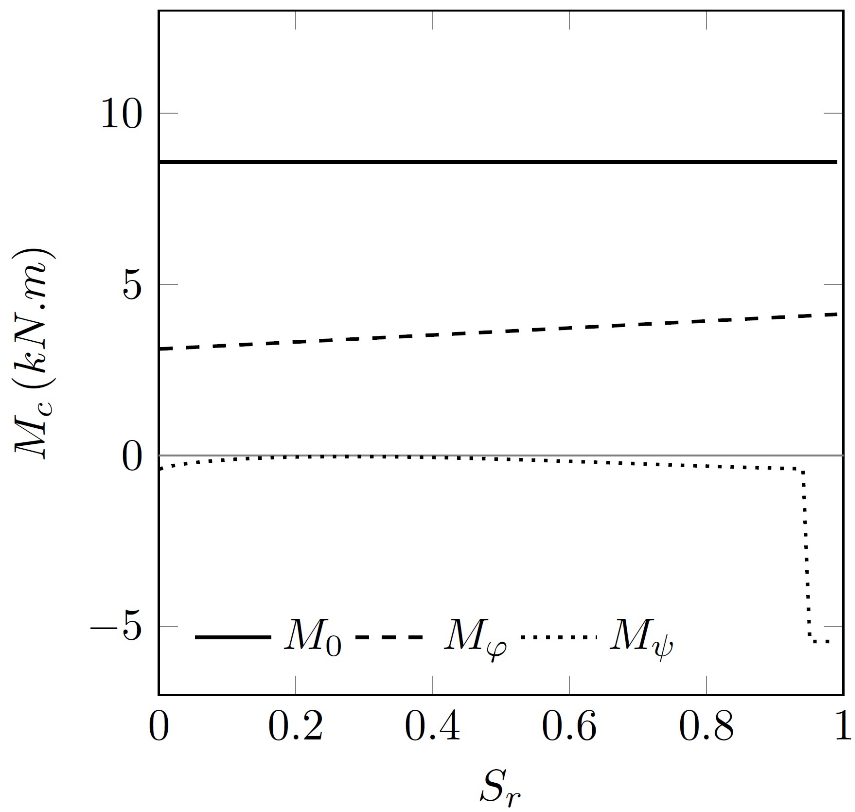

Figure 12: Representation of the components of the resisting moment for a water table level $\mathcal{WT}$ = -0.40 m.